第 34 卷第 6 期　　红 外 与 毫 米 波 学 报　　Vol. 34, No. 6
2015 年 12 月　　J. Infrared Millim. Waves　　December, 2015

文章编号：1001－9014(2015)06－0673－07　　DOI:10.11972/j.issn.1001－9014.2015.06.007

A gradient-based steering kernel reconstruction strategy for semi-random Fourier measurements in compressed remote sensing

DONG Jiang-Shan[1], YIN Jing-Yuan[1,2*], LI Cheng-Fan[1]

(1. School of Computer Engineering and Science, Shanghai University, Shanghai 200444, China;
2. Earthquake Administration of Shanghai Municipality, Shanghai 200062, China)

Abstract: A gradient-based steering kernel (GradSK) reconstruction strategy for compressed remote sensing is proposed. It aims to solve the artifacts and blurriness caused by the none-strictly sparsity and the noisy Fourier undersamples. Semi-random Fourier measurements are presented for encoding, which can preserve approximating components of images and retain the incoherence by random undersamples in the periphery of K-space. The steering kernel derived from multistep gradients is exploited to encapsulate with finite-difference Total Variance (TV) in the unconstrained convex framework for decoding. Numerical results demonstrate the superior performance of this algorithm in the case of noiseless and noisy measurements for compressed remote sensing.

Key words: compressed sensing, Fourier measurements, image reconstruction, steering kernel
PACS: 07.05.Pj

基于梯度转向核的半随机傅里叶域压缩重构算法

董江山[1]，尹京苑[1,2*]，李成范[1]
(1. 上海大学 计算机工程与科学学院,上海　200444; 2. 上海市地震局,上海　200062)

摘要:针对压缩遥感过程中非严格稀疏和傅里叶域欠采样噪声导致的伪影和混叠现象,提出了基于梯度转向核的压缩重构策略(GradSK).在压缩感知编码过程中提出了半随机傅里叶测量的方式,既保留图像的概要分量,同时保证了K-空间随机欠采样的非连贯性.在压缩感知解码过程中提出了由基于多阶梯度的转向核与有限差分总方差(TV)结合的方法,来解决解码过程中的无约束凸框架问题.实验表明,该方法在解决无噪采样和有噪采样的过程中均有较好性能.

关　键　词:压缩感知;傅里叶测量;图像重构;转向核

中图分类号:TP751.41　　**文献标识码**:A

Introduction

Compressed sensing (CS) is a recently proposed theory that allows the reconstruction of a signal sampled in violation of traditional Nyquist criterion. It has been applied to remote sensing, medical imaging, information coding, astrospectroscopy *et. al*. For traditional remote sensing, millions of pixels have to be sampled to formulate a high resolution image. It brings challenges to the sensors and sampling systems. Furthermore, the storage space is a limited resource in the remote sensing platform. Therefore, image data need to be compressed before transmission, and then decompressed at each receiver station. As a result, large number of data have to be discarded, and inevitable distortions occur during the compression and decompression procedures.

Compressed remote sensing (CRS) optimizes the flows of data acquisition and image processing, which combines sampling and compression into linear undersampled measurements. Likewise, CS reveals that a compressible unknown signal can be recovered from incomplete linear measurements by particularly designed nonlinear reconstructions. Accordingly, the number of

---

Received date: 2014-09-30, **revised date**: 2015-10-07　　**收稿日期**:2014-09-30, **修回日期**:2015-10-07

Foundation items: National Natural Science Foundation of China (41404024), Young Teachers Training and Supporting Plan in Shanghai Universities (2014-2016, ZZSD14025)

Biography: DONG Jiang-Shan (1981-), male, Hubei province. Ph. D. degree. Research fields concerns remote sensing image processing. E-mail: jiangshandong@hotmail.com

* **Corresponding author**: E-mail: doubleson@126.com

measurements in CRS is far fewer than those required by traditional sensors. The potential advantage of CRS is that remote sensing instruments can work in low light conditions, and demands for less cost, i. e. power consumptions, sensor sizes, sampling and compression systems and so on. Up to now, the most representative design of CRS is the single-pixel digital camera presented by Baraniuk *et. al*[1] of Rice University, utilizing the DMD as the random binary measurements in spatial domain. Another type of CRS is spatially modulated image Fourier transform spectrometer[2] that randomly measured in Fourier domain. Limited sensors in parallel Fourier-domain imaging are utilized to achieve higher resolutions that traditional imaging cannot reach. Compared with the spatial CRS, Fourier measurements can save the imaging time. The crucial step of CS is the nonlinear reconstruction of ill-posed underdetermined linear inverse problem. State-of-the-art reconstruction algorithms have been proposed recently to solve the problem, such as orthogonal matching pursuit (OMP)[3-4], iterative hard thresholding (IHT)[5-6] and gradient-based algorithms[7]. The OMP algorithm recovers images by choosing the column of measurement matrices that is most strongly correlated with the remaining parts of image matrices. Therefore, the performance closely relies on the selected measurement matrices and the number of samples. IHT method is quite easily to be implemented through iterations. It has been not widely applied due to its slow convergence and the hard selection for thresholds. Gradient projection recovery algorithm poses an unconstrained convex optimization problem and exploits total variation (TV)[8] as the sparsifying transform. While these approaches yield a significant reduction in the sample numbers, the performance is likely to be affected by the approximate sparsity and the noisy measurements.

In this letter, we propose a so-call GradSK recovery strategy for incomplete Fourier remote sensing systems. For sake of compromise between incoherence and robustness to noise, the semi-random scheme is proposed to undersample the Fourier coefficients, which choose samples randomly with density scaling according to 2-D function. Therefore, most energy in the main lobe of function can be preserved to construct the approximate components of images, and the incoherence between sparsifying matrices and the measurement matrices is remained by the random undersamples in the periphery of K-space. Integrated with the semi-random Fourier measurements, we encapsulated both the TV and local structural regularity into the iterative reconstruction framework and optimized the reconstruction by using the gradient descent method. In the prior terms, steering kernel[9] is employed for the local structure regularity of natural remote sensing images, which preserves the edges and reduces the blurriness for noisy measurements. The experiment results indicate that GradSK with the noiseless and noisy semi-random Fourier measurements achieves substantial performance gains compared with its counterparts.

1 Gradient-based steering kernel recovery (GradSK)

1.1 Problem formulation in compressed remote sensing

The problem of estimating N-dimensional original data $\boldsymbol{X}$ can be formulated mathematically as an inverse problem ($K < < N$), where-dimensional measurements $\boldsymbol{Y}$ collected by a compressed remote sensing imaging system are represented as follows:

$$\boldsymbol{Y} = \boldsymbol{\Phi X} + \varepsilon \quad , \quad (1)$$

where ε denotes the possible measurement errors or noises, and compressed optical measurements are described as $K \times X$ measurement matrix $\boldsymbol{\Phi}$.

The CS theory asserts that it is possible to recover sparse images from a small number of random measurements in time or Fourier domain 0[11]. However, most remote sensing images are taken from large field of views, so that the complex scenes in remote sensing images bring about non-sparse in a variety of cases. Therefore, $\boldsymbol{X}$ should be denoted as the K-dimensional sparse data α in sparse basis transform $\boldsymbol{\Psi}$, i. e., $\boldsymbol{X} = \boldsymbol{\Psi}\alpha$ s. t. $\|\alpha\|_{l0} = K \times N$, where $\|\alpha\|_{l0}$ returns the number of nonzero elements. If the measurement matrix $\boldsymbol{\Phi}$ and sparsifying transform $\boldsymbol{\Psi}$ satisfy the Restricted Isometry Property (RIP), the reconstruction can be regarded as solving L1 minimization problem:

$$\min_{\alpha} \|\alpha\|_{l_1} \text{ s. t. } \|\boldsymbol{Y} - \boldsymbol{\Phi\Psi}\alpha\|_{l2} < \varepsilon \quad . \quad (2)$$

Several CS architectures for practical optical imaging systems have been developed recently[12-13]. Figure 1 illustrates one of such representative approaches with spatial light modulation, whereby the aperture modulates the light in the image' Fourier plane. The measurements in Fourier domain refer to the random undersampling F_s for Fourier coefficients $\mathcal{J}$ called K-sparse space, i. e. $\boldsymbol{\Phi} = {}_{f_s} = F_s(\mathcal{J}_{\Omega})$. Accordingly, the reconstruction is obtained by solving the unconstrained Lagrangian as follows:

$$\tilde{\boldsymbol{X}} = \arg\min_{X} \|\boldsymbol{Y} - \mathcal{J}_{f_s}\boldsymbol{X}\|_{l_2} + \lambda \|\boldsymbol{\Psi X}\|_{l_1} \quad . \quad (3)$$

The accuracy of CS reconstruction is generally affected by two factors: (1) The general objects of interest in remote sensing images are approximating sparser rather than strictly sparser, even in the basis of sparsifying transform $\boldsymbol{\Psi}$; (2) The measurements have to be interfered with noises more or less, as a result of the limited precisions of sensors. Most recovery strategies for compressed remote sensing imaging would be degraded or even failed with the noisy measurements. Therefore, the reconstruction strategies robust to perturbations in measurements are demanded imperatively.

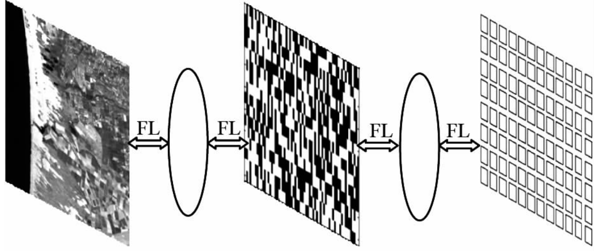

Fig. 1 Compressive sensing camera architectures in Fourier domain
图1 傅里叶域压缩感知成像示意图

1.2 Gradient-based Steering Kernel Reconstruction For Semi-random Fourier Measurements

Most existed measurement matrices are derived from the random Fourier measurements, which are considered to achieve more incoherence for almost all sparsifying transforms. The greater incoherence between measurement matrix $\boldsymbol{\Phi}$ and sparsifying transform $\boldsymbol{\Psi}$, the fewer measurements are required. However, most blind reconstructions with completely random measurements cannot obtain expected performance since of approximate sparsity or noisy measurements, no matter in spatial or Fourier domain. As we all know, most energy of images is concentrated close to the K-space origin in Fourier domain, as shown in Fig. 2(b). These observations show that, for a better performance with remote sensing images, one should be undersampled less near the K-space origin and more in the periphery of K-space. Therefore, semi-random undersampling in Fourier domain is proposed in this paper.

One may choose samples randomly with sampling density scaling according to 2-D function. All of the Fourier coefficients in the main lobe of function are sampled, so that most energy can be preserved to construct the approximate components of images. Meanwhile, other coefficients of side lobes are randomly undersampled with the probability density function . The parameters related to the desired resolution of CRS are set to be 0.05 and 0.8, respectively.

$$F_s(\mathcal{J}_\Omega) = \begin{cases} \mathrm{rand}(0/1) & ,\mathrm{sinc}(a\mathcal{J}_\Omega) < \sigma \\ 1 & ,\mathrm{sinc}(a\mathcal{J}_\Omega) \geqslant \sigma \end{cases} \quad . \qquad (4)$$

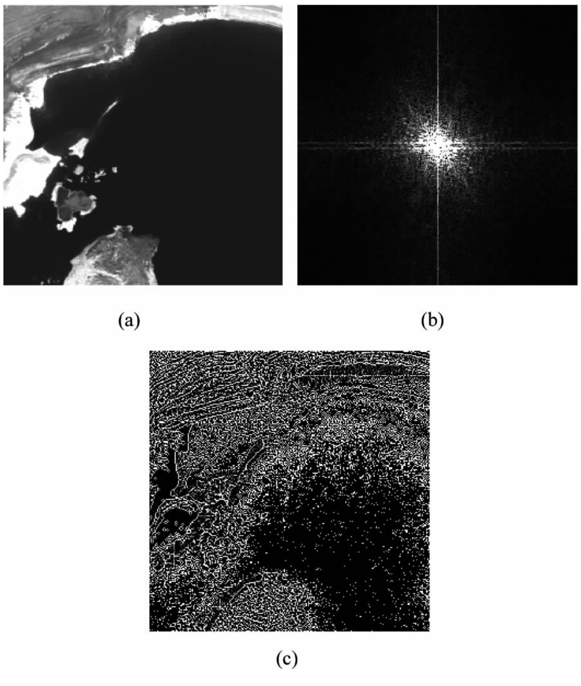

Fig. 2 Landsat TM band 5 image. (a) Original remote sensing image of Landsat TM Band 5, (b) Fourier spectrum, (c) Total variance (TV)
图 2 Landsat TM 传感器波段 5 图像 (a)原始遥感图像, (b)傅里叶谱, (c)有限差分总方差

In the decoding step, a new gradient-based reconstruction approach so-called Gradient based Steering Kernel (GradSK) is presented, while total variation (TV) and steering kernel smoothness is taken as the regularization. Instead of reconstructing by raw pixels, we exploited the steering kernel as the constraint in the TV minimization solving for semi-random Fourier measurements. The steering kernel indicates that pixels on the same side of edges have much stronger relevance than pixels on different sides. Therefore, the regularization term of steering kernel for flat areas can spread to reduce the noise effects, while for texture areas it is able to restrain the blurriness and preserve the details.

$$\boldsymbol{X} = \arg\min_{X} \{ \|\boldsymbol{Y} - \mathcal{J}_\Omega \boldsymbol{X}\|_{l_2}^2 + \lambda \|\boldsymbol{X}\|_{TV} + \gamma \|X - E_{st}(\boldsymbol{X})\|_{l_2}^2 \} \quad , \qquad (5)$$

where $\|\boldsymbol{Y} - \mathcal{J}_\Omega \boldsymbol{X}\|_{l_2}^2$ satisfies the global undersamples in Fourier domain, and the second term $\|\boldsymbol{X}\|_{TV}$ minimizes TV semi norm to recover edges. The third term $E_{st}(\boldsymbol{X})$ for iterations is described as

$$\begin{aligned} E_{st}(\boldsymbol{X}) &= \arg\min_{X} (\boldsymbol{X} - \boldsymbol{PX})^{\mathrm{T}} \boldsymbol{W}^K (\boldsymbol{X} - \boldsymbol{PX}) \\ &= (\boldsymbol{P}^{\mathrm{T}} \boldsymbol{W}^K \boldsymbol{P})^{-1} \boldsymbol{P}^{\mathrm{T}} \boldsymbol{W}^K \boldsymbol{X} \end{aligned} \quad . \qquad (6)$$

The weighted matrix $\boldsymbol{W}^K$ is denoted according to lexicographic orders of x_{ij}^K. And the $\boldsymbol{C}_{ij}$ is the symmetric gradient covariance at , which structures the local kernels.

$$w_{ij}^K(x - x_{ij}) = \frac{\sqrt{\det(\boldsymbol{C}_{ij})}}{2\pi h_k^2} \exp\left\{ -\frac{(x_{ij} - x)^{\mathrm{T}} \boldsymbol{C}_{ij} (x_{ij} - x)}{2h_k^2} \right\} \quad . \qquad (7)$$

In Eq. 7, h_k^2 is the smoothing parameter. $\boldsymbol{P}$ represents the gradient polynomial, and vech(•) operator stands for an operation to stack the lower triangular part of a matrix into a column vector.

$$\boldsymbol{P} = \begin{bmatrix} 1 & (x_{ij} - x)^{\mathrm{T}} & \mathrm{vech}^{\mathrm{T}}\{(x_{ij} - x)(x_{ij} - x)^{\mathrm{T}}\} \\ \cdots & \cdots & \cdots \end{bmatrix} \quad . \qquad (8)$$

Therefore, combing all of terms together, we can get the reconstruction by solving

$$\begin{aligned} \tilde{\boldsymbol{X}} = \arg\min_{X} \{ & \|\boldsymbol{Y} - \mathcal{J}_\Omega \boldsymbol{X}\|_{l_2}^2 + \lambda \|\boldsymbol{X}\|_{\mathrm{TV}} \\ & + \gamma \|[\boldsymbol{I} - (\boldsymbol{P}^{\mathrm{T}} \boldsymbol{W}^K \boldsymbol{P})^{-1} \boldsymbol{P}^{\mathrm{T}} \boldsymbol{W}^K] \boldsymbol{X}\|_{l_2}^2 \} \end{aligned} \quad . \qquad (9)$$

The optimization of Eq. 9 can be effectively addressed by using the gradient descent method[14-15], i.e.,

$$\tilde{\boldsymbol{X}}^{k+1} = \tilde{\boldsymbol{X}}^k - \mu^k \nabla f(\tilde{\boldsymbol{X}}^k) \quad , \qquad (10)$$

where μ^k is the step size of iterations, and the gradient of cost function $\nabla f(\boldsymbol{X})$ is computed as follows:

$$\begin{aligned} \nabla f(\boldsymbol{X}) = {} & 2\mathcal{J}_\Omega^* (\mathcal{J}_\Omega \boldsymbol{X} - \boldsymbol{Y}) + \lambda \nabla \|\boldsymbol{X}\|_{\mathrm{TV}} \\ & + 2\gamma [\boldsymbol{I} - (\boldsymbol{P}^{\mathrm{T}} \boldsymbol{W}^K \boldsymbol{P})^{-1} \boldsymbol{P}^{\mathrm{T}} \boldsymbol{W}^K]^2 \boldsymbol{X} \end{aligned} \quad . \qquad (11)$$

The gradient of total variance $\nabla \|\boldsymbol{X}\|_{\mathrm{TV}}$ is defined as:

$$\begin{aligned} \nabla \|\boldsymbol{X}\|_{\mathrm{TV}} = {} & \frac{d_{i,j}^h + d_{i,j}^v}{\sqrt{(d_{i,j}^h)^2 + (d_{i,j}^v)^2}} - \frac{d_{i-1,j}^v}{\sqrt{(d_{i-1,j}^h)^2 + (d_{i-1,j}^v)^2}} \\ & - \frac{d_{i,j}^h}{\sqrt{(d_{i,j-1}^h)^2 + (d_{i,j-1}^v)^2}} \end{aligned} \quad , \qquad (12)$$

where the derivatives of $\boldsymbol{X}$ along the horizontal and vertical directions are respectively denoted as $d_{i,j}^h(x) = x_{i,j} - x_{i,j+1}$, $d_{i,j}^v(x) = x_{i,j} - x_{i+1,j}$.

2 Numerical experiment and analysis

In this section, gradient-based steering kernel recovery algorithm is compared with L1TV and IHT for simulation of compressed remote sensing imaging in Fourier domain. The tested images are chosen from remote sensing datasets, including Landsat TM and AVIRIS. In these experiments, relative error (RE)[5] and peak signal to noise ratio (PSNR) are used to measure the performance of four algorithms. They are defined as:

$$\mathrm{RE}=\frac{\|\boldsymbol{X}-\tilde{\boldsymbol{X}}\|_2^2}{\|\boldsymbol{X}\|_2^2},\mathrm{PSNR}=10\ \lg\left[\frac{(2^8-1)^2}{\|\boldsymbol{X}-\tilde{\boldsymbol{X}}\|_2^2}\right]\quad,\qquad(13)$$

where is defined as $\boldsymbol{X}$ and $\tilde{\boldsymbol{X}}$.

2.1 GradSK for various samplings in Fourier domain

CS measurements are generated by applying Fourier transform for each test image, and then the Fourier coefficients are partially undersampled according to the sampling schemes. The compression proportion is determined by the ratio of measurement numbers (RMN)0. Figure 3 (a-0)-(c-0) show the semi-random and another two representative sampling scheme patterns, i. e. random sampling and radial sampling. The '1' locations in the binary patterns are reserved, while the '0' locations are discarded. In this experiment, we compared the performance of GradSK with the three sampling schemes by setting RMN = 30%. The images reconstructed by GradSK in noiseless cases are presented in Fig. 3(a-1)-(c-1). For the noisy cases, Gaussian noises with variance $\sigma=1$ and $\sigma=10$ are added into both the real and imaginary parts of Fourier coefficients, which are demonstrated in Fig. 3(a-2)-(c-2) and Fig. 3(a-3)-(c-3), respectively. Both of the radial and semi-random sampling schemes

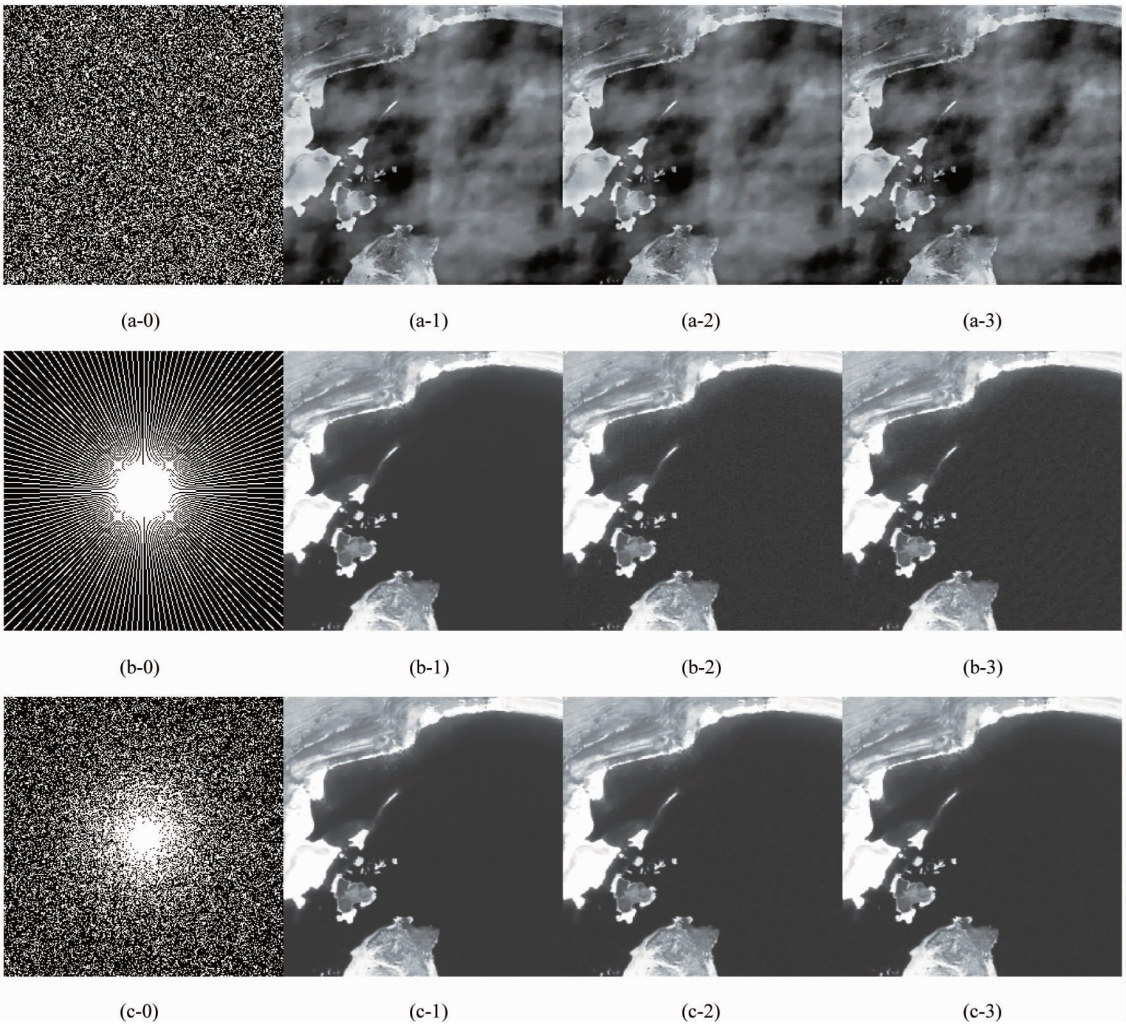

Fig. 3 GradSK with representertive sampling schemes. (a-0 ~ 3) random sampling scheme pattern and reconstructed images with Gaussian noises $\sigma=0$, $\sigma=1$, $\sigma=10$; (b-0 ~ 3) radial sampling scheme pattern and reconstructed images with Gaussian noises $\sigma=0$, $\sigma=1$, $\sigma=10$; (c-0 ~ 3) semi-random sampling scheme pattern and reconstructed images with Gaussian noises $\sigma=0$, $\sigma=1$, $\sigma=10$

图3 基于梯度转向核的压缩重构策略的采样方案(a-0 ~ 3)高斯噪声为 $\sigma=0$, $\sigma=1$, $\sigma=10$ 的随机采样方案及重构图像 ,(b-0 ~ 3)高斯噪声为 $\sigma=0$, $\sigma=1$, $\sigma=10$ 的径向采样方案及重构图像,(c-0 ~ 3)高斯噪声为 $\sigma=0$, $\sigma=1$, $\sigma=10$ 的半随机采样方案及重构图像

outperform random sampling at the small RMN for noiseless measurements, since texture information is preserved by sampling most of high frequency Fourier coefficients. Figure 3(b-2) and (b-3) indicate that the radial sampling is more sensitive to the measurement noise than the proposed semi-random. The absence of randomness in radial sampling schemes causes the artifacts in the noisy cases.

2.2 Comparison with other three reconstruction algorithms

We generated the noiseless and noisy test sets for comparison with ZerosFill, IHT and L1TV. In both tests, we set $\lambda = \gamma = 0.01$ for all GradSK reconstructions, and the initial reconstruction starts from zeros for IHT.

In the noiseless test, twenty remote sensing images are reconstructed from only 10% to 50% RMN in the increments of 5% without measurement noise. Figure 4 demonstrates the performance of four algorithms considering 40% noiseless measurements. Figure 4(a) depicts the recovery result using direct zeros-filling reconstruction. In IHT reconstruction shown in Fig. 4(b), sym8 wavelet is used for the basis of sparsity, while the initial thresholding value is set to 0.06. Figure 4(c) demonstrates the reconstruction of L1TV. According to the relative error images, the reconstruction of L1TV suffers from artifacts, despite better than ZerosFill and IHT. And the proposed GradSK is superior to others especially in the rich texture. Figure 6(a) shows the corresponding RE as the RMN increases. It is clear from the statistic curves that IHT performs a slightly better than other three algorithms while $RMN \leqslant 25\%$. With the increasing of RMN from 25%, the reconstructed images of GradSK are closer to the original ones, benefitting from the steering kernel constraints.

The second experiment is very similar in nature except that the real and imaginary parts of Fourier coefficients are interfered with $\sigma = 0.1$ Gaussian noise. Figure 5 gives the $RMN = 40\%$ set of reconstructed images as the demonstration for noisy measurements. The images of the second and third rows in Fig. 5 are partially enlarged views of the reconstructions. The images recovered by ZerosFill and IHT respectively shown in Fig. 5(a) and (b) are blurred by the noisy measurements. Not all weaker components below the threshold in Fourier domain can be recovered during the iterations of IHT. Figure 5(d) demonstrates the reconstruction of the proposed GradSK, which preserves much more edges than L1TV shown in Fig. 5(c). As shown in Fig. 6(b), after the RMN of about 0.28, L1TV performs a slightly more robust to noise than IHT. And GradSK outperforms all the other algorithms in terms of the statistic PSNR. It can be seen from Fig. 6(a) and (b) that RE and PSNR of the four algorithms can be improved with the increased RMN. L1TV and GradSK expand their advantage on relatively adequate samples.

Table 1 illustrates the average runtime of four algorithms for the noiseless and noisy image sets. The iterative approximation is the most time-consuming for gradient-based methods, so that the direct reconstruction ZerosFill runs much faster than other three iterative algorithms. More measurements would lead to more storage and runtimes, but it does not scale linearly with time complexity as shown in Table 1.

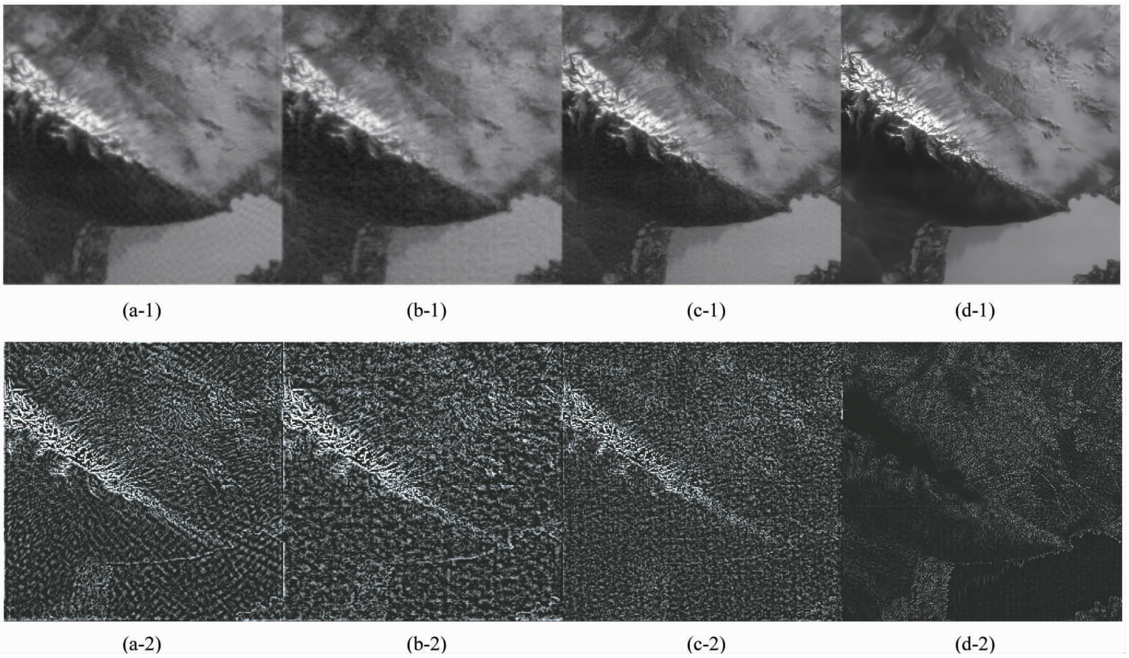

Fig. 4 Reconstructed images and RE for noiseless measurements with RMN = 40%. (a) ZerosFill, RE = 0.116, (b) L1TV, RE = 0.052, (c) IHT, RE = 0.034, (d) GradSK, RE = 0.025
图 4 $RMN = 40\%$ 时无噪采样的重构图像及相对误差 (a) ZerosFill, 相对误差 = 0.116, (b) L1TV, 相对误差 = 0.052, (c) IHT, 相对误差 = 0.034, (d) GradSK, 相对误差 = 0.025

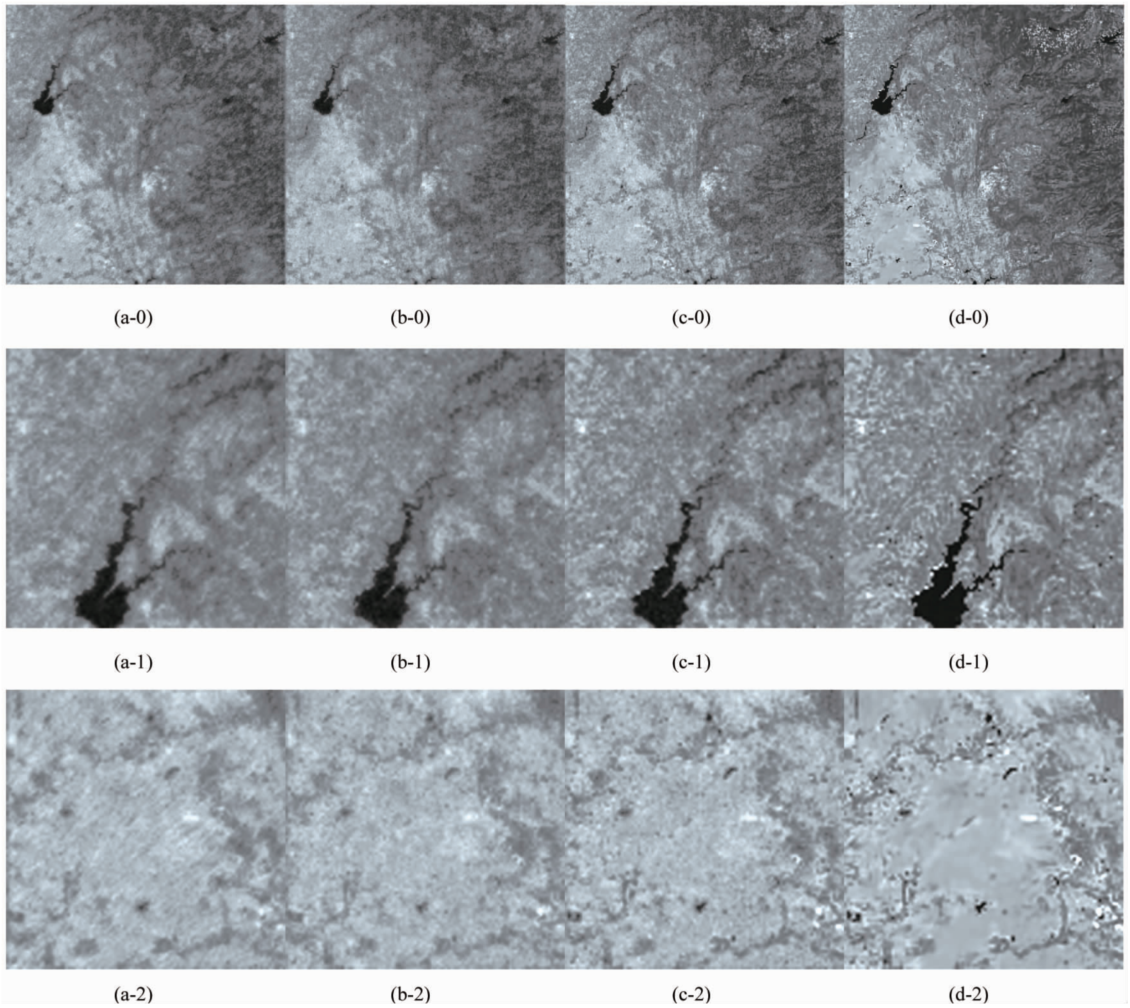

Fig. 5 Reconstructed images and enlarged views for noisy measurements with *RMN* = 40%. (a-0 ~ 2) ZerosFill, PSNR = 28.75 (b-0 ~ 2) L1TV, PSNR = 44.36 (c-0 ~ 2) IHT, PSNR = 50.36 (d-0 ~ 2) GradSK, PSNR = 48.95

图 5 RMN = 40% 时无噪测量的重构图像及放大视图 (a-0 ~ 2) ZerosFill, 峰值信噪比 = 28.75, (b-0 ~ 2) L1TV, 峰值信噪比 = 44.36, (c-0 ~ 2) IHT, 峰值信噪比 = 50.36, (d-0 ~ 2) GradSK, 峰值信噪比 = 48.95

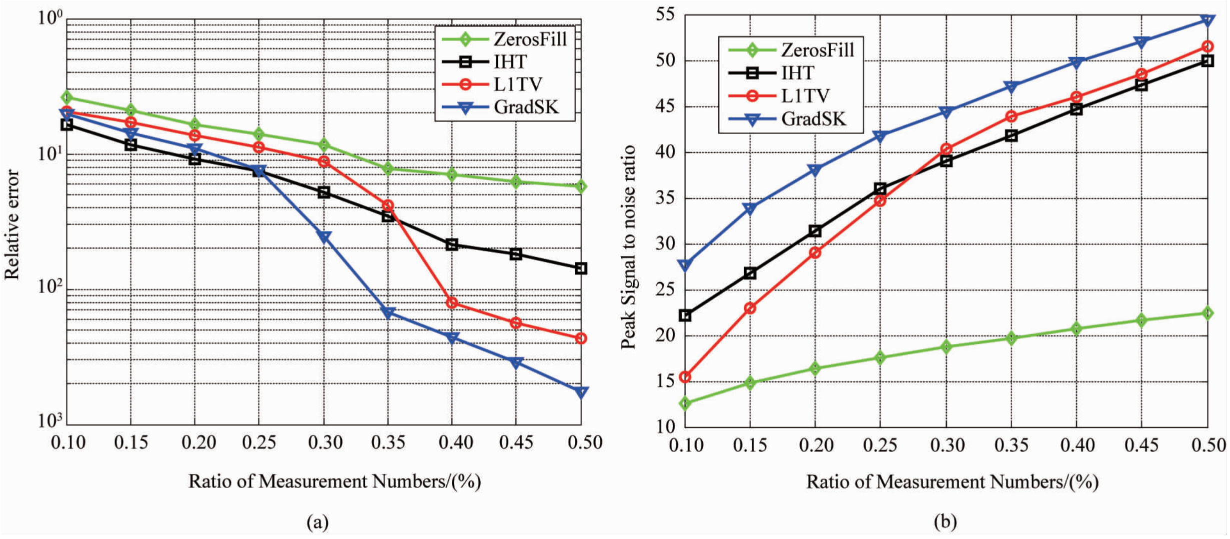

Fig. 6 Performance comparison of four algorithms when statistic RE with different RMN, (a) noiseless measurements. (b) measurements

图 6 不同采样数字比情况下四种算法的性能比较 (a) 无噪采样的相对误差统计, (b) 有噪采样的峰值信噪比统计

Table 1 Average runtime of four algorithms
表 1 四种算法的平均运算时间

Runtime(sec)	ZerosFill	IHT	L1TV	GradSK
Noiseless + 30% RMN	0.736	1.532	2.683	2.924
Noiseless + 50% RMN	1.245	2.744	4.521	5.013
Noisy +30% RMN	0.749	1.646	4.873	5.230
Noisy +50% RMN	1.232	2.789	7.358	8.106

3 Conclusion

It is a well known fact that the performance of compressed reconstructions is affected by the approximating sparsity of images and the perturbations in measurements, which is often the case in remote sensing imaging systems. In this letter, GradSK recovery strategy for semi-random Fourier measurements is proposed. Semi-random in Fourier domain for encoding is exploited to sample randomly with density scaling according to 2-D function. Most energy concentrated in the main lobe is preserved, while the random undersamples are employed in the periphery of K-space. For compressed decoding, remote sensing images are sparsified by TV. Meanwhile, the steering kernel estimation is taken as the prior term to preserve edges. TV and the steering kernel estimation are encapsulated for decoding in the framework of L1 minimization. Compared with ZerosFill, IHT and L1TV algorithms, the experiments of the noiseless and noisy cases indicate that the proposed method offers improvement in reconstruction quality and more robustness for CRS.

References

[1] Duarte M, Davenport M. Takhar D, *et al*. Single-pixel imaging via compressive sampling[J]. *IEEE Signal Processing Magazine*, 2008, **25**(2): 83 -91.

[2] Lustig M, Donoho D, Pauly J M. Sparse MRI: The application of compressed sensing for rapid MR imaging[J]. *Magnetic Resonance in Medicine*, 2007, **58**(6): 1182 -1195.

[3] Needell D, Vershynin R. Signal recovery from incomplete and inaccurate measurements via regularized orthogonal matching pursuit [J]. *IEEE Journal of Selected Topics in Signal Processing*, 2010, **4**(2): 310 -316.

[4] Tropp J, Gilbert A. Signal recovery from random measurements via orthogonal matching pursuit[J]. *IEEE Transactions on Information Theory*, 2007,**53**(12):4655 -4666.

[5] Beck A, Teboulle M. A fast iterative shrinkage-thresholding algorithm for linear inverse problems[J]. *SIAM Journal on Imaging Sciences*, 2009, **2**(1): 183 -202.

[6] Blumensath T, Davies M. Iterative hard thresholding for compressed sensing[J]. *Applied and Computational Harmonic Analysis*, 2009, **27**(3): 265 -274.

[7] Patel V M, Maleh R, Gilbert A C. Gradient-based image recovery methods from incomplete fourier measurements[J]. *IEEE Transaction on Image Processing*, 2012, **21**(1): 94 - 105.

[8] Wang Y, Yang J, Yin W, *et al*. A new alternating minimization algorithm for total variation image reconstruction[J]. *SIAM Journal on Imaging Sciences*, 2008,**1**(3): 248 -272.

[9] Takeda H, Farsiu S, Milanfar P. Kernel regression for image processing and reconstruction[J]. *IEEE Transaction on Image Processing*, 2007,**16**(2): 349 -366.

[10] Ma J. Improved iterative curvelet thresholding for compressed sensing and measurement[J]. *IEEE Transaction on Instrumentation and Measurement*, 2011,**60**(1):126 - 136.

[11] YANG Yang, LIU Ze, ZHANG Meng. A new undersampling image reconstruction method based on total variation model[J]. *Journal of Infrared and Millimeter Wave*(杨扬,刘哲,张萌. 一种基于全变差模型的欠采样图像重构方法,**红外与毫米波学报**) 2012, **31**(2): 153 -158.

[12] Willett R M, Marcia R F, Nichols J M. Compressed sensing for practical optical imaging systems: a tutorial [J]. *Optical Engineering*, 2011, **50**(7), 072601 -14.

[13] ZHAO Ming, AN Bo-Wen, WANG Yun, *et al*. A multi-channel multiplexing compressive remote sensing approach based on non-local similarity constraint [J]. *J. Infrared Millim. Waves* (赵明,安博文,王运,等.基于非局部相似度约束的多通道复用压缩遥感成像方法,**红外与毫米波学报**) 2015, **34**(1): 122 -127.

[14] Wu Y, Xiao C, Ding Z, *et al*. Linear precoding for finite alphabet signaling over MIMOME wiretap channels[J]. *IEEE Trans. Veh. Technol.*, 2012, **61**(7): 2599 -2612.

[15] Wu Y, Wang M, Xiao C, *et al*. Linear precoding for MIMO broadcast channels with finite-alphabet constraints [J]. *IEEE Trans. Wireless Commun.*, 2012, **11**(8): 2906 -2920.